PROCEEDINGS OF SPIE

SPIEDigitalLibrary.org/conference-proceedings-of-spie

# Comparative study of the optical properties of colon mucosa and colon precancerous polyps between 400 and 1000 nm

Sónia Carvalho, Nuno Gueiral, Elisabete Nogueira, Rui Henrique, Luís Oliveira, et al.

SPIE.

# Comparative study of the optical properties of colon mucosa and colon precancerous polyps between 400 and 1000 nm

Sónia Carvalho [a], Nuno Gueiral [b,c], Elisabete Nogueira [b,c], Rui Henrique [a,d], Luís Oliveira [b,c], Valery V. Tuchin [e,f,g]

[a] Portuguese Oncology Institute of Porto, Department of Pathology and Cancer Biology and Epigenetics Group-Research Centre, Rua Dr. António Bernardino de Almeida S/N, Porto, Portugal, 4200-072 Porto; [b] Polytechnic of Porto, School of Engineering, Physics Department, Rua Dr. António Bernardino de Almeida, nº 431, 4200-072 Porto, Portugal; [c] Centre of Innovation in Engineering and Industrial Technology, ISEP, Rua Dr. António Bernardino de Almeida, nº 431, 4200-072 Porto, Portugal; [d] Department of Pathology and Molecular Immunology, Institute of Biomedical Sciences Abel Salazar – University of Porto (ICBAS-UP), Rua de Jorge Viterbo Ferreira, nº 228, 4050-313 Porto, Portugal; [e] Saratov National Research State University, Research-Educational Institute of Optics and Biophotonics, 83 Astrakhanskaya str., 410012 Saratov, Russia; [f] Precision Mechanics and Control Institute of the Russian Academy of Sciences, Laboratory of Laser Diagnostics of Technical and Living Systems, 24 Rabochaya, 410028 Saratov, Russia; [g] National Research Tomsk State University, Interdisciplinary Laboratory of Biophotonics, 36 Lenin's av., 634050 Tomsk, Russia

## ABSTRACT

Optical properties of biological tissues are unique and may be used for tissue identification, tissue discrimination or even to identify pathologies. Early stage colorectal cancer evolves from adenomatous polyps that arise in the inner layer of the colorectal tube – the mucosa. The identification of different optical properties between healthy and pathological colorectal tissues might be used to identify different tissue components and to develop an early stage diagnosis method using optical technologies. Since most of the biomedical optics techniques use light within the visible and near infrared wavelength ranges, we used the inverse adding-doubling method to make a fast estimation of the optical properties of colorectal mucosa and early stage adenocarcinoma between 400 and 1000 nm. The estimated wavelength dependencies have provided information about higher lipid content in healthy mucosa and higher blood content in pathological tissue. Such data has also indicated that the wavelength dependence of the scattering coefficient for healthy mucosa is dominated by Rayleigh scattering and for pathological mucosa it is dominated by Mie scattering. Such difference indicates smaller scatterer size in healthy mucosa tissue. Such information can now be used to develop new diagnosis or treatment methods for early cancer detection or removal. One possibility is to use optical clearing technique to improve tissue transparency and create localized and temporary tissue dehydration for image contrast improvement during diagnosis or polyp laser removal. Such techniques can now be developed based on the different results that we have found for healthy and pathological colorectal mucosa.

**Keywords:** Inverse Adding Doubling method, absorption coefficient, scattering coefficient, reduced scattering coefficient, scattering anisotropy factor, human colorectal tissues, adenomatous polyps, cancer

## 1. INTRODUCTION

The development of new diagnostic or treatment methods with application in the various fields of clinical practice is strongly based on mathematical models that describe light propagation and interaction inside the biological tissues.[1-3] Such models can be constructed once the fundamental optical properties of tissues are known.[1] Optical diagnostic and treatment methods work at different wavelengths within the optical spectral range,[2-3] meaning that the optical properties

Dynamics and Fluctuations in Biomedical Photonics XIV, edited by Valery V. Tuchin, Kirill V. Larin, Martin J. Leahy, Ruikang K. Wang, Proc. of SPIE Vol. 10063, 100631L · © 2017 SPIE
CCC code: 1605-7422/17/$18 · doi: 10.1117/12.2253023

of tissues need to be known for a wide range of wavelengths. Since cheap and fast indirect methods for estimating the optical properties of biological tissues were made available,[4-5] several publications have emerged that present the optical properties of biological tissues for some particular wavelengths[2-3,6-9] or for some wavelength ranges.[10-11] Only more recently extended wavelength dependence of the optical properties has become a concern amongst researchers. In more recent papers large wavelength ranges have been considered to present the optical properties of various biological tissues. Some of the tissues that have already been studied for large spectral ranges are the colon,[1] brain, breast, skin, muscle and heart tissues,[12] peritoneal tissues,[13-14] and skin, subcutaneous and mucous tissues.[15]

It has been already demonstrated that the optical properties can also be used to distinguish native from coagulated liver tissues,[16] between healthy and pathological breast[17-19] and skin tissues.[20] This possibility of discriminating between healthy and pathological tissues is highly significant if optical methods are to be developed for diagnosis and treatment procedures. Considering the uniqueness of the optical properties of healthy and pathological tissues, it is highly recommended that their evaluation should be made for the various tissues and pathologies to gather knowledge for future developments.

Biological tissues are heterogeneous materials that contain diverse components such as proteins, cells, water, blood, lipids, etc. Fortunately, the absorption spectra for the most of these tissue components are known and available.[21] Consequently, by evaluating the absorption coefficient ($\mu_a$), the scattering coefficient ($\mu_s$), the reduced scattering coefficient ($\mu'_s$) or the anisotropy factor ($g$) for a particular tissue, one can evaluate the presence of these tissue components by identifying their bands. The wavelength dependence for the scattering coefficients ($\mu_s$ and $\mu'_s$) in biological tissues is described in literature.[1, 12-13, 15] Typically, biological tissues present a combination between Rayleigh and Mie scattering terms, as described by Eq. (1):[12]

$$\mu_s(\lambda) = a' \times \left( f_{Ray} \left( \frac{\lambda}{500(nm)} \right)^{-4} + (1 - f_{Ray}) \times \left( \frac{\lambda}{500(nm)} \right)^{-b_{Mie}} \right) \tag{1}$$

Equation (1) is written to express the wavelength dependence of $\mu_s$, but same equation is used to model the wavelength dependence of $\mu'_s$. The difference between the two wavelength dependencies for the same tissue is the value that parameters in Eq. (1) assume.[12] The usual wavelength dependence for the other basic optical properties of biological tissues is also known. The absorption coefficient, in particular, does not have a typical equation to describe its wavelength dependence, but it is known that it decreases strongly between approximately 400 and 500 nm, and it maintains almost constant low values after that. Usually a peak is seen around 550 nm, due to the presence of blood in the tissues.[13] The anisotropy factor usually increases in an exponential manner with wavelength for visible and near-infrared wavelengths. This is one of the various equations used to describe such behavior:[13]

$$g(\lambda) = a + b \times \left( 1 - e^{\left( -\frac{\lambda - c}{d} \right)} \right). \tag{2}$$

A relation between the anisotropy factor and the scattering coefficients ($\mu_s$ and $\mu'_s$) is also known. The following equation allows for calculation of $\mu'_s$ from $\mu_s$ and g: [2,13]

$$\mu'_s(\lambda) = \mu_s(\lambda) \times (1 - g(\lambda)). \tag{3}$$

If we have means of estimating all the optical properties of a tissue with the exception of one of those in Eq. (3), this property can be calculated.

Considering the indirect methods for optical property estimation, the inverse Monte Carlo (IMC)[4] and the inverse Adding-Doubling (IAD)[5] are the most popular and accurate. Usually, these methods use a combination of three optical measurements obtained from a tissue sample to estimate a set of three optical properties for that tissue. As referred in literature,[13] the estimation of the optical properties is more precise if we use the IMC technique, but the IAD method needs less computational time to generate a solution of the inverse problem.

Considering these indirect methods for estimating the optical properties of biological tissues and since we were already studying human colorectal healthy and pathological tissues for other purposes, we decided to estimate the wavelength dependence of their optical properties between 400 and 1000 nm.

The third most common cancer and the fourth to cause cancer-related mortality worldwide is colorectal carcinoma, with a 50% mortality rate of the 1.2 million new cases each year.[22] To establish a reliable diagnosis, colorectal endoscopy[23] is necessary and colectomy constitutes the basis of surgical treatment, eventually complemented with chemotherapy and/or radiotherapy.[24] To turn diagnosis/treatment procedures easier and less aggressive to the patient, non-invasive optical methods are desired. For this reason, it is highly important to detect and evaluate differences in the optical properties of the healthy and pathological colorectal tissues.

Colon and rectum are tube-like structures composed of several layers from the inside to the outside as represented in Figure 1.

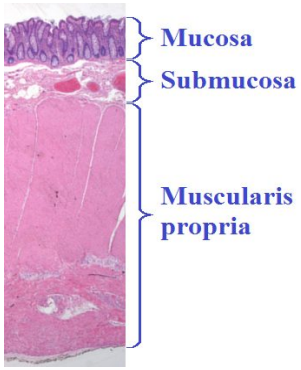


Figure 1. Structure of the colorectal wall containing histologically distinct layers – from the inside (lumina) outwards: mucosa, submucosa and *muscularis propria*.

Adenomatous polyps, which are the precursor lesions of colorectal adenocarcinoma, originally develop in the innermost colorectal layer – the mucosa.[25] Not removing these polyps at this early stage implies that they will evolve into adenocarcinoma which intrudes the other layers that compose the colorectal wall, first in the submucosa and eventually reaching the *muscularis propria*, the subserosal tissue or even the peritoneal lining or adjacent organs.[26] Since the polyps like the one presented in Figure 2 start developing in the mucosa, endoscopic instrumentation can be inserted into the lumen to detect them.[23]

Figure 2. Colorectal polyp viewed in a surgical specimen.

As can be seen in Figure 2, the adenomatous polyp shows a more intense red color than the surrounding tissue suggesting that it might have higher blood content. The internal composition of colorectal mucosa and polyps is certainly different and consequently the optical properties of these tissues will also present different values. Early in 2016, a research group has demonstrated that colorectal mucosa and dysplastic colorectal tissues present different refractive index (RI) values at 964 nm.[27] To estimate the optical properties of both colorectal tissues in a wide wavelength range, we also had to measure the wavelength dependencies of their RI.[28] We have observed that the wavelength dependence of the RI is similar for the healthy and pathological colorectal mucosa, but pathological tissue presents higher values.

In addition to the RI measurements, we have also measured the total transmittance ($T_t$), total reflectance ($R_t$) and collimated transmittance ($T_c$) from healthy and pathological colorectal tissues. Considering all these measurements, we have performed fast IAD simulations for various wavelengths between 400 and 1000 nm to estimate the wavelength dependencies of the optical properties and check if they present differences for the two types of tissues.

The methodology and results obtained are presented in sections 2 and 3, respectively. In section 3 we will compare between the results obtained from healthy and pathological tissues and in section 4 we will present our perspectives for future research in this filed.

## 2. MATERIALS AND METHODS

As indicated above, our objective was to study the wavelength dependencies of the optical properties of healthy and pathological colorectal tissues to evaluate differences. To perform this study, we have performed various measurements from samples that were surgically removed from patients under treatment at the Portuguese Oncology Institute of Porto, Portugal. The methodology used in this study is described in detail in the following sub-sections.

### 2.1 Tissue samples

All the tissue samples used in this study were collected from patients that have signed a written consent previous to surgical procedures allowing for subsequent use of surgical specimens for diagnostic and research purposes. Such procedure was approved by the Ethics Committee of the Portuguese Oncology Institute of Porto. These patients were 9 men and 3 women with ages ranging from 43 to 94.

After surgical procedures, healthy and pathological colorectal mucosa samples were separated and preserved frozen at −80 ºC for a period of 12 to 24 hrs. A cryostat from Thermo Scientific™ (Waltham, Massachusetts, USA), model Microm HM 550 was used to prepare samples with circular form ($\phi$=1 cm) and 0.5 mm thickness. Samples were kept in saline for 10 min before initiating studies, to mimic natural hydration.

### 2.2 Measurements

To perform the inverse simulations, several measurements were necessary. We have performed four types of spectral measurements and RI measurements from the two types of tissues. Considering the spectral measurements, we have acquired $T_c$, $T_t$ and $R_t$ spectra from three healthy and three pathological mucosa tissues. All these spectra range from 400 to 1000 nm.

Additionally to the spectral measurements, the RI of healthy and pathological tissues was obtained for several individual wavelengths between 400 and 1000 nm,[28] using the internal reflection method.[29-31] The RI study of healthy and pathological colorectal tissues also produced interesting results and we have submitted this study for publication recently.[28] In that study, we have also measured from three individual healthy and three individual pathological samples for each of the following laser wavelengths: 401.4, 532.5, 589.6 (Abbe refractometer), 668.1, 782.1, 820.8 and 850.7 nm. These measurements were averaged and the two wavelength dependencies for healthy and pathological tissues were fitted with a curve described by the Cornu equation (Eq. (4)):[31-32]

$$RI(\lambda) = A + \frac{B}{(\lambda - C)}. \quad (4)$$

When fitting the mean RI data of both healthy and pathological colorectal mucosa tissues with Eq. (4), different values for A, B and C were obtained for each case.

All the data collected from the spectral and RI measurements was used in the simulations to estimate the optical properties of healthy and pathological mucosa tissues.

### 2.3 IAD simulations

To estimate the wavelength dependencies of the optical properties of healthy and pathological colorectal tissues, we have used the IAD code available at the Oregon Medical Laser Centre website.[5,21] Such code is not as accurate as the IMC code[4] as referred in literature,[13] but it allows for fast estimations of the optical properties with small error. Each simulation with the IAD code takes approximately 2−3 s to estimate the optical properties. Since the code performs a simulation that corresponds to an individual wavelength, we had to perform several simulations to estimate the optical properties for various wavelengths between 400 and 1000 nm. We have selected a wavelength resolution of 25 nm. Considering that we have made an inverse simulation that corresponds to each 25 nm between 400 and 1000 nm, a total of 25 simulations were made to obtain complete wavelength dependence for all four optical properties. Since we wanted to obtain three complete wavelength dependencies for each optical property per tissue type, we performed a total of 150 simulations. Averages of the results from the three simulations for case were calculated.

Considering each individual simulation, the IAD code works by using as input the values of $T_t$, $T_c$ and $R_t$, along with the RI of the sample and media above and below the sample. Sample thickness is also required. After the simulation ends, the optical properties $\mu_a$, $\mu'_s$ and $g$ are generated. Using Eq. (3) we calculated $\mu_s$ from $\mu'_s$ and $g$.

The generated results from these simulations are presented in section 3, showing the differences between healthy and pathological colorectal tissues.

## 3. RESULTS AND DISCUSSION

Since the objective of our study consists on identifying differences between the optical properties of human healthy and pathological colorectal tissues, we will begin by presenting the wavelength dependencies of the RI of these tissues.

In our previous research,[28] we have estimated the mean wavelength dependencies for the RI of healthy and pathological colorectal tissues. As can be seen from Figure 3, pathological mucosa shows higher RI values than healthy mucosa in all the wavelength range from 400 to 1000 nm.

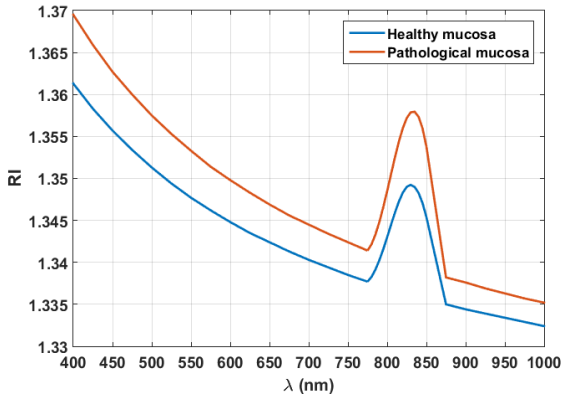


Figure 3. Wavelength dependence for the RI of human colorectal healthy and pathological mucosa.

It is important to stress that apart from the peaks observed around 825 nm, the two wavelength dependencies in Figure 3 are described by a Cornu equation (Eq. (4)). When performing the fitting of mean experimental data, for healthy (*hm*) and for pathological mucosa (*pm*) we obtained the following values:

$$RI(\lambda)_{hm} = 1.315 + \frac{16.73}{(\lambda - 38.84)}, \tag{5}$$

$$RI(\lambda)_{pm} = 1.315 + \frac{19.25}{(\lambda - 46.83)}. \tag{6}$$

To create the curves presented in Figure 3, we have used our experimental data measured for wavelengths between 400 and 850 nm. The remaining of the curves between 850 and 1000 nm were calculated based on the fact that colorectal mucosa obeys the same decreasing behaviour for wavelengths above 900 nm as for lower wavelengths, as indicated in literature.[27] The non-monotonic behaviour observed for the two tissues around 825 nm is evidence that both types of tissues contain lipids. As we can see from Figure 4, lipids present some absorption peaks in the same spectral range:

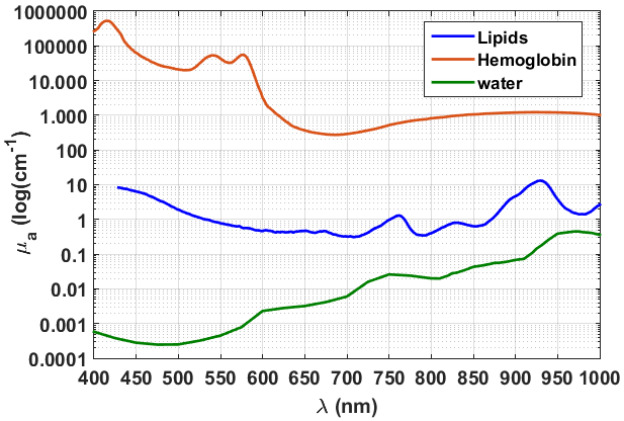


Figure 4. Absorption coefficient spectra of water, hemoglobin and lipids (data taken from the Oregon Medical Laser Centre website[21]).

In figure 4 we see the wavelength dependencies for the absorption coefficient spectra of haemoglobin,[33] water[34] and lipids.[35] Considering the spectra for lipids (blue line in figure 4), we see three absorption peaks: the first at 762 nm, the second at 830 nm and the third at 930 nm. The peak at 830 nm is very close to the 825 nm that we observe in Figure 3. Authors of Ref. 35 have used pig lard in their studies to obtain the absorption coefficient spectrum presented in Figure 4. In our case, we studied human colorectal tissues freshly collected from patients. Pig lard is pure fat for this reason we see three absorption peaks in Figure 4. Human colorectal tissues contain different components and consequently we could see only the peak at 825 nm in Figure 3.

Using the RI data presented for both tissues in Figure 3 along with spectral measurements of $T_t$, $T_c$ and $R_t$ that we have acquired, we performed three complete simulations for healthy mucosa and other three for pathological mucosa. Averaging the results, we have obtained the mean wavelength dependencies for the four optical properties of healthy and pathological mucosa. The mean and standard deviation bars for the absorption coefficient spectra of healthy and pathological mucosa are presented in Figure 5:

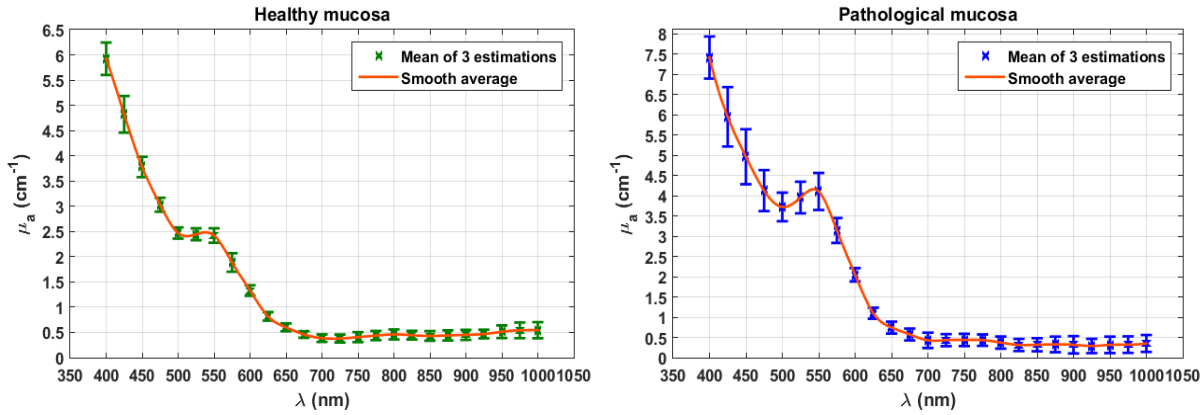


(a) (b)

Figure 5. Absorption coefficient spectra of healthy (a) and pathological (b) human colorectal mucosa.

Considering the wavelength dependence for healthy mucosa presented in Figure 5(a), we see that it shows the same behaviour and levels of values as the data reported in Ref. 1. Pathological mucosa shows same type of wavelength dependence, but for wavelengths lower than 650 nm, it presents values a little higher than healthy mucosa. Another difference that we can see when comparing the two graphs in Figure 5 concerns the peak at 550 nm that corresponds to haemoglobin absorption – pathological mucosa shows a more intense peak than healthy mucosa, indicating that pathological tissues have more blood content. To compare between the data obtained for the two types of tissues we have represented the smooth curves in both graphs of Figure 5 in a single graph in Figure 6.

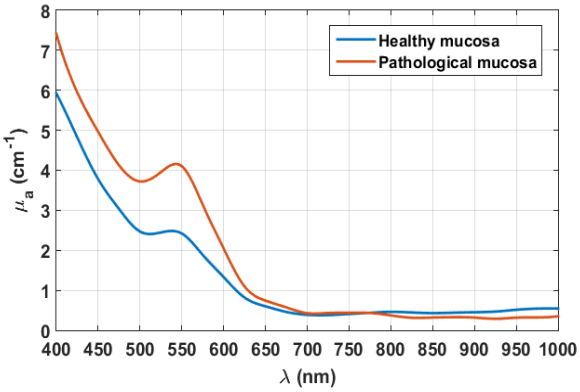


Figure 6. Mean smooth wavelength dependence of the absorption coefficient for healthy and pathological mucosa.

Figure 6 shows that for wavelengths below 700 nm, the pathological mucosa shows higher absorption than healthy mucosa. Above 700 nm pathological mucosa shows lower values, but very approximated to the ones estimated for healthy mucosa, indicating that for this range the absorption coefficient tends to be constant and with very low values.

Regarding the reduced scattering coefficient, Figure 7 contains the mean estimated data, the standard deviation bars, the smooth curve that fits the mean data (green line) and the theoretical line (in orange) that describes the wavelength dependence according to literature (Eq. (1)):[12]

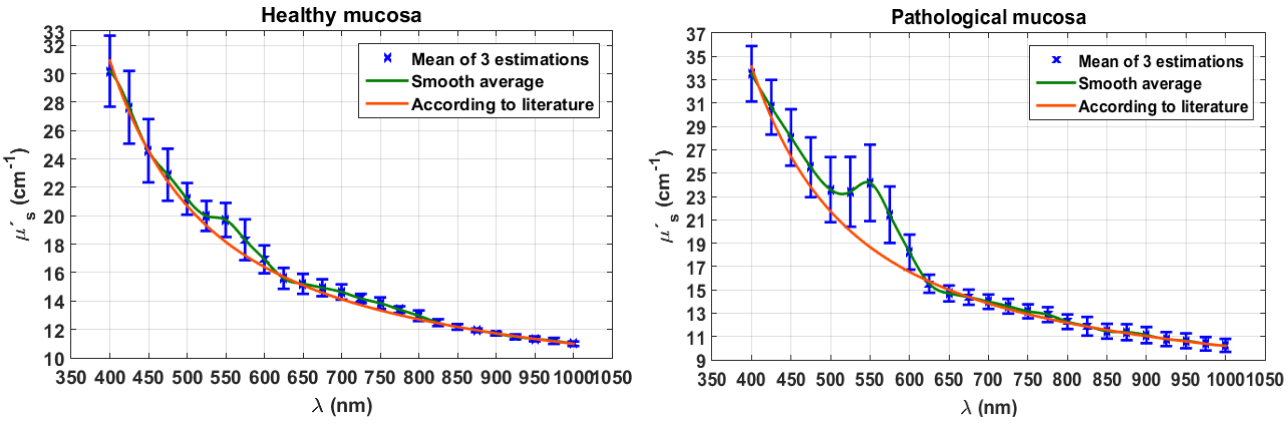


(a) (b)

Figure 7. Reduced scattering coefficient spectra of healthy (a) and pathological (b) human colorectal mucosa.

Comparing our data for the healthy mucosa with the data presented in Ref. 1, we see that our estimations originated smaller values for $\mu'_s$. The reason for this discrepancy can be the origin of the samples used in the two studies, since the samples used in the study of Ref. 1 were collected from Russian patients. Another reason is related to the fact that we have used only IAD simulations to estimate the optical properties and the authors of Ref. 1 have used IAD as a first estimation and then used the IMC code to obtain more accurate results.[1] Nevertheless, since we have estimated all data for the optical properties of healthy and pathological colorectal mucosa using the IAD code, the same level of precision is observed for the two tissues and a comparison can be made. Analysing the data of graphs of Figure 7, we see that for both tissues the mean generated data have a peak at 550 nm. Once again this peak is evidence of blood content in the tissues, since haemoglobin presents absorption bands in this range (see Figure 4). Figure 7 indicates once again that pathological mucosa has more blood content than healthy mucosa, since the peak at 550 nm is more intense in Figure 7

(b). Additionally to the peak observed at 550 nm, we see another peak around 750 nm for both tissues. This peak is evidence of the lipid content in mucosa tissues and it seems from graphs in Figure 7 that healthy mucosa has more lipid content than pathological mucosa. To calculate the theoretical curves that fit $\mu'_s(\lambda)$ for both tissues (orange curves of graphs of Figure 7), we have neglected the data of the peaks that correspond to blood and lipids. For healthy mucosa the mean data fitting with a curve described by Eq. (1) has obtained by using MATLAB's CFTOOL and the parameters for that fitting are the ones presented in:

$$\mu'_{s-hm}(\lambda) = 20.7 \times \left( 0.287 \times \left( \frac{\lambda}{500(nm)} \right)^{-4} + (1 - 0.287) \times \left( \frac{\lambda}{500(nm)} \right)^{-0.4752} \right) \quad . \tag{7}$$

The R-square value obtained for this fitting was 0.9996. A similar fitting was made for the mean $\mu'_s$ data of the pathological mucosa. The resulting equation for this fitting is:

$$\mu'_{s-pm}(\lambda) = 21.73 \times \left( 0.3325 \times \left( \frac{\lambda}{500(nm)} \right)^{-4} + (1 - 0.3325) \times \left( \frac{\lambda}{500(nm)} \right)^{-0.5752} \right) \tag{8}$$

The R-square value obtained in this fitting was 0.9982. To have an idea how the wavelength dependencies obtained for $\mu'_s$ of both tissues differ one from the other we created the graph in Figure 8 with both theoretical curves described by Eqs. (7) and (8).

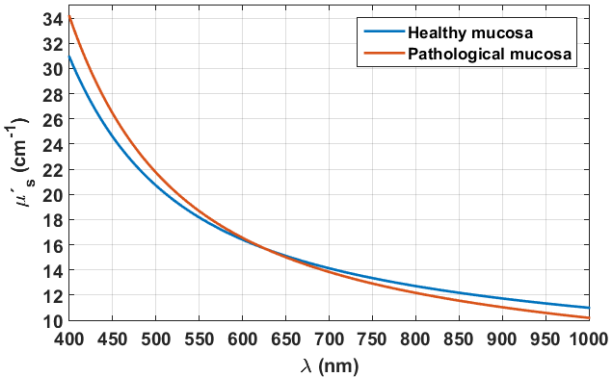


Figure 8. Wavelength dependence for $\mu'_s$ of healthy and pathological mucosa.

From Figure 8 we see that both tissues show similar levels of $\mu'_s$. At lower wavelengths than 625 nm, pathological mucosa presents higher values than healthy mucosa and for longer wavelengths the opposite is observed. Nevertheless, both curves are much approximated in this spectral range, meaning that $\mu'_s$ does not allow for pathology discrimination.

The third optical property generated by the IAD simulations was *g*. Similarly to the graphs presented in Figure 7 for $\mu'_s$, we have represented in Figure 9 the mean estimated data for *g*, the standard deviation bars, the smooth curve that fits the mean data points (green line) and the theoretical line (in orange) that describes the wavelength dependence according to literature.[13]

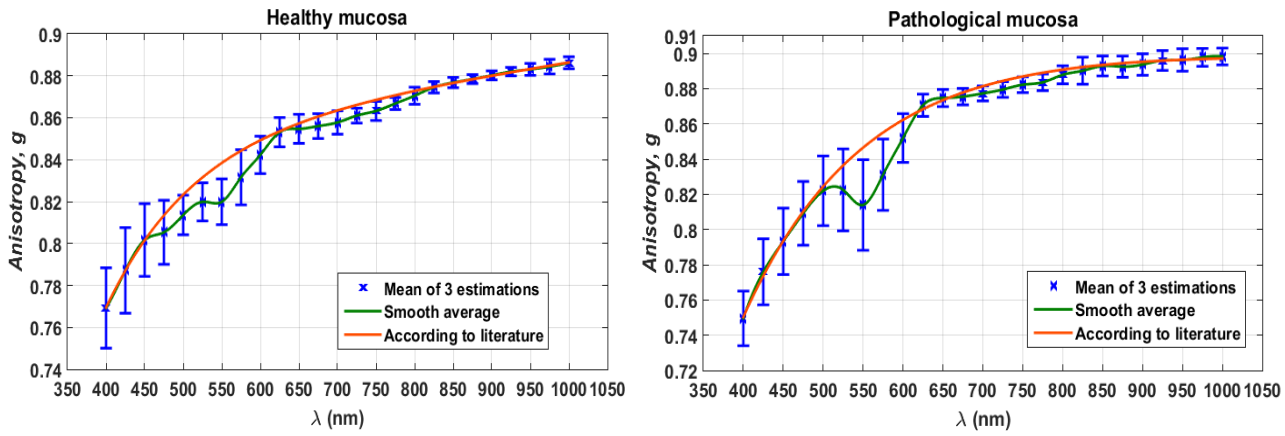


(a) (b)

Figure 9. Anisotropy factor spectra of healthy (a) and pathological (b) human colorectal mucosa.

Comparing our data for the healthy mucosa in figure 9 (a) with the data presented by authors of Ref. 1, we see once again that our estimations have produced lower values for $g$. Despite the difference in values, the wavelength dependence is the same – increasing $g$ with wavelength. Similarly to the analysis that we have made for $\mu'_s$, we see that the wavelength dependencies represented in both graphs of figure 9 show some bands that correspond to haemoglobin (around 550 nm) and lipids (around 750 nm). Both tissues show these evidences. The band for haemoglobin is more intense in pathological mucosa, showing that pathological tissue has more blood content than healthy tissue. The evidence of lipids, on the other hand, seems to be a little stronger in healthy mucosa tissue, confirming the information retrieved from graphs of $\mu'_s$ (Figure 7).

To calculate the curves that describe the increasing behaviour of $g$ with wavelength that is described in literature[1,12] (orange curves in graphs of Figure 9), we had to neglect the estimated points that correspond to the bands of haemoglobin and lipids. The calculated curves that provide the best fittings of the mean $g$ data are presented in Eqs. (9) and (10) for healthy and pathological mucosa, respectively:

$$g_{hm}(\lambda) = 0.8311 \times e^{6.494\times10^{-5}\lambda} - 2.634 \times e^{-8.628\times10^{-3}\lambda} \quad , \tag{9}$$

$$g_{hm}(\lambda) = 0.9088 \times e^{9.681\times10^{-6}\lambda} - 2.189 \times e^{-6.619\times10^{-3}\lambda} \quad . \tag{10}$$

The R-square values obtained when fitting the mean g data in graphs of Figure 9 with Eqs. (9) and (10), was 1 for healthy mucosa and 0.9984 for pathological mucosa.

To compare between both types of tissue, we have represented the curves described by Eqs. (9) and (10) in Figure 10.

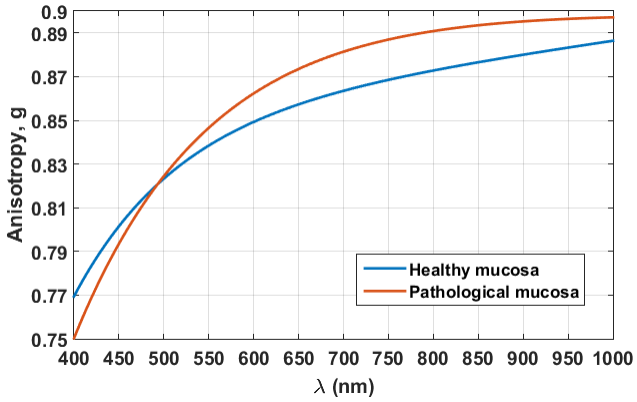


Figure 10. Anisotropy factor spectra of healthy and pathological mucosa.

Figure 10 shows that the wavelength dependence for the anisotropy factor is very similar for the two types of tissues, with much approximated levels in this spectral range. We see also that anisotropy is higher for healthy mucosa at wavelengths smaller that approximately 500 nm and for wavelengths above this value pathological mucosa shows higher values.

Finally, and considering the estimated values for $\mu'_s$ and $g$, we have used Eq. (3) to calculate the wavelength dependence for $\mu_s$. This calculation was made for three sets of $\mu'_s$ and $g$ data for healthy mucosa and for three sets of $\mu'_s$ and $g$ data for pathological mucosa. Figure 11 presents the mean wavelength dependencies for $\mu_s$ obtained in these calculations for healthy and pathological mucosa.

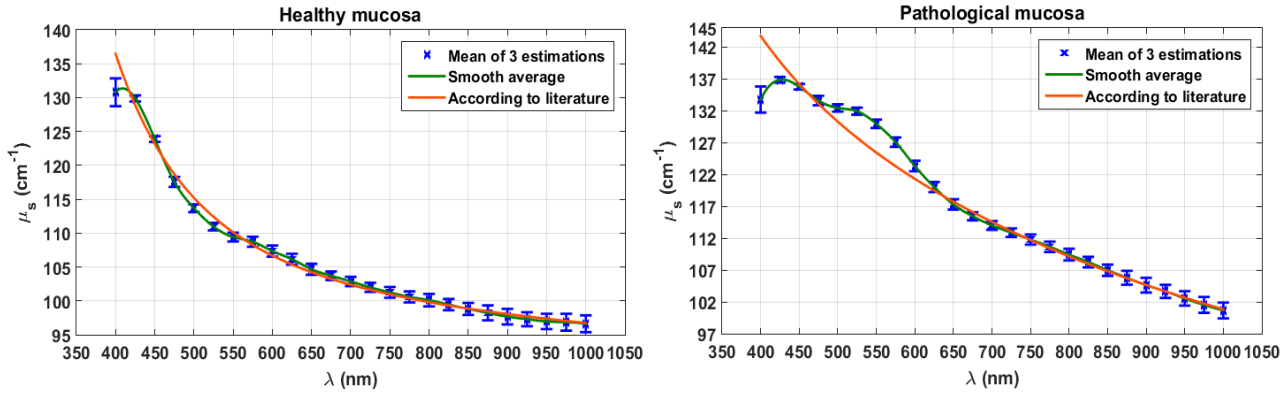


(a) (b)

Figure 11. Scattering coefficient spectra of healthy (a) and pathological (b) human colorectal mucosa.

The two graphs in Figure 11 contain the mean calculated data, the standard deviation bars, the smooth curve that connects the data (green line) and the theoretical curve described in literature[12] and according to Eq. (1) (orange line).

Comparing the data for healthy mucosa presented in graph of figure 11(a) with the data from Ref. 1, we observe once again that our estimated data is low, but shows the correct wavelength dependence. Even more, our data shows a dip at lower wavelengths as it is seen in data on Ref. 1 for $\mu_s$. Comparing between healthy and pathological mucosa we see that pathological mucosa shows clear evidence of blood content, since the graph in figure 11(b) contains a peak around 550 nm. This peak corresponds to haemoglobin absorption band (see Figure 4) and it is not seen in graph of Figure 11(a). Such data confirms the assumption that we made when visualizing Figure 2 – adenomatous polyps contain more blood.

The curves that are presented in literature[12] to fit the decreasing wavelength dependence of $\mu_s$ (orange curves in graphs of Figure 11) were calculated according to Eq. (1). To calculate these curves, we had to neglect the dip observed at 400 – 425 nm for both tissues and the data that corresponds to haemoglobin absorption in the case of pathological mucosa. The orange curves in graphs of Figure 11 are described by Eqs. (11) and (12), for healthy and pathological mucosa, respectively:

$$\mu_{s-hm}(\lambda) = 115.2 \times \left( 0.1161 \times \left( \frac{\lambda}{500(nm)} \right)^{-4} + (1 - 0.1161) \times \left( \frac{\lambda}{500(nm)} \right)^{-0.08636} \right), \tag{11}$$

$$\mu_{s-pm}(\lambda) = 130.3 \times \left( 0.01654 \times \left( \frac{\lambda}{500(nm)} \right)^{-4} + (1 - 0.01654) \times \left( \frac{\lambda}{500(nm)} \right)^{-0.3479} \right). \tag{12}$$

The R-square values obtained when fitting the mean $\mu_s$ data in graphs of Figure 11 with Eqs. (11) and (12) was 0.9941 for healthy mucosa and 0.9988 for pathological mucosa. To make a comparison between the two types of tissues for the $\mu_s$ we have created the graph in Figure 12 with the two theoretical curves described by Eqs. (11) and (12).

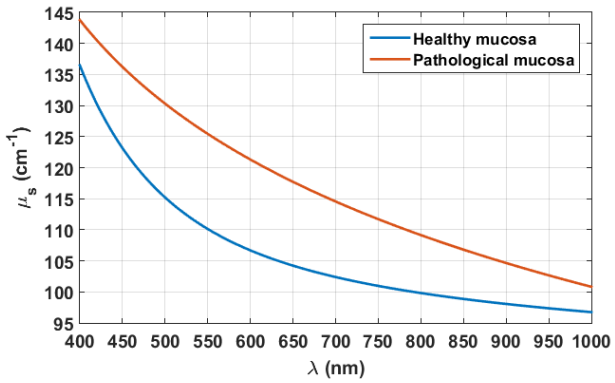


Figure 12. Scattering coefficient spectra of healthy and pathological mucosa.

Figure 12 shows that $\mu_s$ is higher for pathological mucosa all the way between 400 and 1000 nm. Although the levels of values are not strongly different for the two types of tissues, pathological mucosa shows higher level of values and a more linear behaviour than healthy mucosa. Such difference in behaviour can be justified by comparing between Eqs. (11) and (12). Analysing these equations we see that in both cases Mie term dominates, but if for healthy tissue Rayleigh term has 11.6% of inclusion and Mie term increment is – 0.086, for diseased tissue we have only 1.6% of Rayleigh term inclusion and Mie term increment is – 0.35. Such information suggests that bigger sized particles are present in pathological tissue. This argumentation makes sense if we think that cancer cells are complex and big sized structures that were created by mutations.

## 4. CONCLUSIONS AND FUTURE PERSPECTIVES

After analysing and comparing between the estimated data for healthy and pathological colorectal mucosa, we can now evaluate the differences in their optical properties.

From the RI data presented in Figure 3 we saw similar wavelength dependence for healthy and pathological tissue, but higher RI values for pathological tissue. We saw also from the RI data that both tissues present evidence of lipids inside.

Considering the other optical properties and their wavelength dependencies, we have observed similar wavelength dependence for healthy and pathological tissues in almost all cases, with similar levels of values for $\mu_a$, $\mu'_s$ and $g$. In the particular cases of $\mu'_s$ and $g$, we have observed that healthy tissue gives spectral evidence of more lipid content than pathological tissue (see Figure 7). In opposition, pathological tissue has demonstrated spectral evidence in $\mu_a$, $\mu'_s$ and $g$ of more blood content than healthy tissue. In opposition to the similar levels and wavelength dependence between healthy and pathological tissues observed for $\mu_a$, $\mu'_s$ and $g$, $\mu_s$ shows some differences. Comparing the wavelength dependence for this optical property between the two types of tissues (Figure 12) we observe that pathological tissue has higher levels of $\mu_s$ than healthy tissue and more linear wavelength dependence. Such fact can be more accurately interpreted if we observe the Rayleigh and Mie scattering terms in Eqs. (11) and (12). The estimated values seen in these equations demonstrate that healthy mucosa has a higher Rayleigh scattering term inclusion than pathological mucosa, suggesting that diseased tissue contains bigger sized scatterers. Such fact is in agreement with the complex and big-sized structures that are originated in normal cell mutations and culminate in uncontrolled proliferation that gives rise to tumour formation.

Regardless of the somehow poor discriminating information obtained for healthy and pathological colorectal mucosa tissues, the optical properties and their wavelength dependencies are individual for each tissue and the differences, small or high, must be considered when theoretical models are to be developed for treating or diagnosing colorectal cancer.

Our study was based only on IAD simulations and according to literature[1] IMC simulations provide more accurate results in the estimations. Comparing between our results and the data from Ref. 1 for healthy colorectal mucosa, we see indeed that our estimations have provided lower values than the ones estimated with IMC simulations. For the near future, we plan to perform IMC simulations with our measured data to check if our estimations for healthy mucosa approach the values presented in Ref. 1. If such is not verified, we can assume that the nature between our samples (Portugal) and the ones used in study of Ref. 1 (Russia) is different.

In face of the results obtained with this study, we plan to use same methodology with tissues from other anatomical areas to check if values of the optical properties or their wavelength dependence are somehow different and allow for pathology discrimination. Considering that we have observed different lipid and blood content in colorectal healthy and pathological tissues and also significantly different spectra for $\mu_s$ of these two tissues, we plan to develop a method for isolating spectra of the optical properties of colorectal tissue components. That way we might identify the spectra for the optical properties of cancer cells.

## ACKNOWLEDGEMENTS

The authors appreciate the availability of instrumental and technical resources made available by I3S-Porto and the help of Cláudia Machado in preparing the tissue samples used in these studies.
This research was supported by the Portuguese research grant FCT-UID/EQU/00305/2013.
VVT was supported by the Russian Presidential grant NSh-7898.2016.2, the Russian Governmental grant 14.Z50.31.0004, and The National Research Tomsk State University Academic D. I. Mendeleev Fund Program.

## REFERENCES

[1] Bashkatov, A. N., Genina, E. A., Kochubey V. I., Rubtsov, V. S., Kolesnikova, E. A. and Tuchin, V. V., "Optical properties of human colon tissues in the 350 – 2500 spectral range," Quantum Electronics 44(8), 779-784 (2014).

[2] Tuchin, V. V., [Tissue Optics: Light Scattering Methods and Instruments for Medical Diagnosis], 3rd Ed., SPIE Press, Bellingham (2015).

[3] Vo-Dinh, T., [Biomedical Photonics Handbook], CRC Press, Boca Raton (2003).

[4] Wang, L.-H., Jacques, S. L. and Zheng, L.-Q., "MCML – Monte Carlo modeling of photon transport in multi-layered tissues," Computer Methods and Programs in Biomedicine 47(2), 131-146 (1995).

[5] Prahl, S. A., van Gemert, M. J. C. and Welch, A. J. "Determining the optical properties of turbid media by using the adding-doubling method," Applied Optics 32(4), 559-568 (1993).

[6] Cheong, W.-F., Prahl, S. A. and Welch, A. J., "A review of the optical properties of biological tissues," IEEE J. of Quantum Electronics 26(12), 2166-2185 (1990).

[7] Patterson, M. S., Chance, B. and Wilson, B. C., "Time resolved reflectance and transmittance for the non-invasive measurement of tissue optical properties," Applied Optics 28(12), 2331-2336 (1989).

[8] Pickering, J. W., Bosman, S., Posthumus, P., Blockland, P., Beek, J. F. and van Gemert, M. J. C., "Changes in the optical properties (at 632.8 nm) of slowly heated myocardium," Applied Optics 32(4), 367-371 (1993).

[9] Pickering, J. W., Prahl, S. A., van Wieringen, N. Beek, J. F., Sterenborg, H. J. C. M. and van Gemert, M. J. C., "Double-integrating-sphere system for measuring the optical properties of tissue," Applied Optics 32(4), 399-410 (1993).

[10] Firbank, M., Hiraoka, M., Essenpreis, M. and Delpy, D. T., "Measurement of the optical properties of the skull in the wavelength range 650-950 nm," Phys. Med. Biol. 38(4), 503-510 (1993).

[11] Marchesini, R. Clemente, C., Pignoli, E. and Brambilla, M., "Optical properties of in vitro epidermis and their possible relationship with optical properties of in vivo skin," J. Photochem. Photobiol. B. 16(2), 127-140 (1992).

[12] Jacques, S. L., "Optical properties of biological tissues: a review," Phys. Med. Biol. 58(11), R37-R61 (2013).

[13] Bashkatov, A. N., Genina, E. A., Kozintseva, M. D., Kochubey, V. I., Gorodkov, S. Y. and Tuchin, V. V., "Optical properties of peritoneal biological tissues in the spectral range of 350 – 2500 nm," Optics and Spectroscopy 120(1), 1-8 (2016).

[14] Kozintseva, M. D., Bashkatov, A.N., Kochubey, V. I., Genina, E. A., Gorodkov, S. Y., Morozov, D. A. and Tuchin, V. V. "Optical properties of parietal peritoneum in the spectral range 350 – 2500 nm," Proc. of SPIE 9031 (2014).

[15] Bashkatov, A. N., Genina, E. A., Kochubey, V. I. and Tuchin, V. V., "Optical properties of human skin, subcutaneous and mucous tissues in the wavelength range from 400 to 2000 nm," J. of Phys. D: Appl. Phys 38(15), 2543-2555 (2005).

[16] Germer, C.-T., Roggan, A., Ritz, J. P., Isbert, C., Albrecht, D., Müller, G. and Buhr, H. J., "Optical properties of native and coagulated human liver tissue and liver metastases in the near infrared range," Laser. Surg. Med. 23(4), 194-203 (1998).

[17] Tromberg, B. J., Shah, N., Lanning, R., Cerussi, A., Espinoza, J., Pham, T., Svaasand, L. and Butler, J., "Non-invasive in vivo characterization of breast tumors using photon migration spectroscopy," Neoplasia 2(1-2), 26-40 (2000).

[18] Troy, T. L., Page, D. L. and Sevick-Muraca, E. M., "Optical properties of normal and diseased breast tissues: prognosis for optical mammography," J. Biomed. Opt. 1(3), 342-355 (1996).

[19] Peters, V. G., Wyman, D. R., Patterson, M. S. and Frank, G. L., "Optical properties of normal and diseased human breast tissues in the visible and near infrared," Phys. Med. Biol. 35(9), 1317-1334 (1990).

[20] Solomatina E., Jiang, B., Novak, J. and Yaroslavsky, A. N., "Optical properties of normal and cancerous human skin in the visible and near-infrared spectral range," J. Biomed. Opt. 11(6), 064026-1-9 (2006).

[21] http://omlc.org/spectra/

[22] Brenner, H., Kloor, M. and Pax, C. P., "Colorectal cancer," The Lancet 383(9927), 1490-1502 (2014).

[23] Curran, S. D. and Schwartz, L. H., "Colorectal cancer imaging," in Colorectal Cancer: Evidence-based Chemotherapy Strategies, L. B. Saltz Ed., pp. 219-230, Humana Press, New Jersey, USA (2007).

[24] Lacy, A. M., García-Valdecasas, J. C., Delgado, S., Castells, A., Taurá, P., Piqué, J. M., Visa, J., "Laparoscopy-assisted colectomy versus open colectomy for treatment of non-metastatic colon cancer: a randomized trial," The Lancet 359(9325), 2224-2229 (2002).

[25] Subramaniam, R., Mizoguchi, A. and Mizoguchi, E., "Mechanistic roles of epithelial and immune cell signaling during the development of colitis-associated cancer," Cancer Res. Front. 2(1), 1-21 (2016).

[26] Pierangelo, A., Benali, A., Antonelli, M. R., Novikova, T., Validire, P., Gayet, B. and De Martino, A., "Ex-vivo characterization of human colon cancer by Mueller polarimetric imaging," Opt. Express 19(2), 1582-1593 (2011).

[27] Giannios, P., Koutsoumpos, S., Toutouzas, K. G., Matiatou, M., Zografos, G. C. and Moutzouris, K., "Complex refractive índex of normal and malignant human colorectal tissue in the visible and near-infrared," J. Biophotonics 1-8 (2016).

[28] Carvalho, S., Gueiral, N., Nogueira. E., Henrique, R., Oliveira, L. and Tuchin, V. V., "Wavelength dependence of the refractive índex of human colorectal tissues: comparison between healthy mucosa and cancer," J. Biomed. Phot. & Eng., submitted.

[29] Ye, Q., Wang, J., Deng, Z. C., Zhou, W. Y., Zhang, C. P., Tian and J. G., "Measurement of the complex refractive index of tissue-mimicking phantoms and biotissue by extended differential total reflection method," J. Biomed. Opt. 16(9), 0.97001-1-5 (2011).

[30] Wang, J., Deng, Z., Wang, X., Ye, Q., Zhou W., Mei, J., Zhang, C. and Tian, J., "Measurement of the refractive index of hemoglobin solutions for a continuous spectral region," Biomed. Opt. Express 6(7), 2536-2541 (2015).

[31] Ding, H., Lu, J. Q., Wooden, W. A., Kragel, P. J. and Hu, X. H., "Refractive indices of human skin tissues at eight wavelengths and estimated dispersion relations between 300 and 1600 nm," Phys. Med. Biol. 51(6), 1479-1489 (2006).

[32] Deng, Z., Wang, J., Ye, Q., Sun, T., Zhou, W., Mei, J., Zhang, C., Tian, J., "Determination of continuous complex refractive index dispersion of biotissue based on internal reflection," J. Biomed. Opt. 21(1), 015003 (2016).

[33] Takatani, S., and Graham M. D., "Theoretical analysis of diffuse reflectance from a two-layer tissue model," IEEE Trans. Biomed. Eng. 26(12), 656-664 (1987).

[34] Hale, G. M., and Querry, M. R., "Optical constants of water in the 200 nm to 200 μm wavelength region," Appl. Opt. 12(3), 555-563 (1973).

[35] van Veen, R. L. P., Sterenborg, H. J., Pifferi, A., Torricelli, A., Chikoidze, E. and Cubeddu, R., "Determination of visible-near infrared absorption coefficients of mammalian fat, with time- and spatially resolved diffuse reflectance and transmission spectroscopy," J. Biomed. Opt. 10(5), 054004-1-6 (2005).